Supporting Information

Spontaneous flexoelectricity and band engineering in MS_2 (M=Mo, W) nanotubes

Jiansheng Dong[†], Huamin Hu[†], Hai Li and Gang Ouyang[*]

Key Laboratory of Low-Dimensional Quantum Structures and Quantum Control of Ministry of Education, Key Laboratory for Matter Microstructure and Function of Hunan Province, School of Physics and Electronics, Hunan Normal University, Changsha 410081, China

*Email address: gangouy@hunnu.edu.cn

[†] These authors contributed equally to this work.

Contents

S1. Calculation of Coulomb electrostatic energy of intertube

For case of bilayer MoS_2, the interaction between M-M and M-S can be negligible because the coupling of interlayer between M-M and S-M is far weaker than that of S-S, thus, the electronic coupling of two adjacent layers is mainly determined by the interlayer interaction of S-S. Therefore, the Coulomb electrostatic energy of interlayer can be written as $U_{coul}^{layer} = C\frac{q_S q_S}{r_{S-S}}$, where q_S is the partial electrostatic charges for S atoms, r_{S-S} is the distance of interlayer. Note that we estimate $U_{coul}^{layer} = 0.14$ eV/atom. When a bilayer MoS_2 is rolled into DW NT, the distance of intertube is ~3.44 Å and the Coulomb electrostatic energy is $U_{coul}^{inter} = 0.12$ eV/atom, which is independent on tube diameter. Therefore, the variation of Coulomb electrostatic energy is $\Delta U_{coul}^{inter} = 0.02$ eV/atom. Therefore, the Coulomb electrostatic energy of intertube can be neglected because this part is far weaker than that of bonds potential energy.

S2. Calculation of bond identities under different diameters

In general, monolayer MS_2 is a hexagonal structure, where M layers are sandwiched by two S layers. The bond length $h_0 = \sqrt{\left(\frac{a}{\sqrt{3}}\right)^2 + \left(\frac{c}{2}\right)^2}$, and the bond angles $\cos\theta = 1 - \frac{a^2}{2h_0^2}$ and $\cos\psi = 1 - \frac{c^2}{2h_0^2}$, where a and c are the in-plane lattice parameters at the equilibrium state. θ and ψ are the in-plane and out-of-plane bond angles, respectively. When a monolayer MS_2 is rolled into nanotube (NT), the mirror symmetry will be broken. As a result, the inner part of NT shrinks and its outer part expands. Therefore, the inner and outer parts have same average strain, i.e.,

$\overline{\varepsilon}_{out} = -\overline{\varepsilon}_{in}$. We can further obtain the average strain of the outer part of SW MS_2-NTs

$$\overline{\varepsilon}_{out} = \int_0^{\frac{H}{2}} \frac{2}{H} zKdz = \frac{H}{2D} \tag{S1}$$

where H denotes the thickness of monolayer MS_2, D is the NT diameter. Notably, the relationship between bond identities (bond length and bond angles) and diameter of SW MS_2-NTs satisfies

$$\begin{cases} h_1^{o,i} = \sqrt{\left(\frac{a}{\sqrt{3}}\left(1 \pm \frac{H}{2D}\right)\right)^2 + \left(\frac{H}{2}\left(1 \mp \frac{H \cdot \nu_\perp}{2D}\right)\right)^2} \\ h_2^{o,i} = \sqrt{\left(\frac{a}{2}\left(1 \mp \frac{H \cdot \nu_{//}}{2D}\right)\right)^2 + \left(\frac{a}{2\sqrt{3}}\left(1 \pm \frac{H}{2D}\right)\right)^2 + \left(\frac{H}{2}\left(1 \mp \frac{H \cdot \nu_\perp}{2D}\right)\right)^2} \\ \theta_1^{o,i} = \arccos\left(\frac{h_1^{o,i2} + h_2^{o,i2} - \left(\frac{\sqrt{3}a}{2}\left(1 \pm \frac{H}{2D}\right)\right)^2 - \left(\frac{a}{2}\left(1 \mp \frac{H \cdot \nu_{//}}{2D}\right)\right)^2}{2 \cdot h_1^{o,i2} \cdot h_2^{o,i2}}\right) \\ \theta_2^{o,i} = \arccos\left(1 - \frac{a^2}{2 \cdot h_2^{o,i2}}\left(1 \mp \frac{H \cdot \nu_{//}}{2D}\right)^2\right) \\ \psi_1 = \arcsin\left(\frac{H}{2h_1^o}\left(1 - \frac{H \cdot \nu_\perp}{2D}\right)\right) + \arcsin\left(\frac{H}{2h_1^i}\left(1 + \frac{H \cdot \nu_\perp}{2D}\right)\right) \\ \psi_2 = \arcsin\left(\frac{H}{2h_2^o}\left(1 - \frac{H \cdot \nu_\perp}{2D}\right)\right) + \arcsin\left(\frac{H}{2h_2^i}\left(1 + \frac{H \cdot \nu_\perp}{2D}\right)\right) \end{cases} \tag{S2}$$

where $h_1^{o,i}$, $h_2^{o,i}$, $\theta_1^{o,i}$, $\theta_2^{o,i}$, ψ_1 and ψ_2 denote bond lengths and bond angles induced by curvature, respectively. The superscript *o* and *i* represent the inner and outer parts, $\nu_{//}$ and $\nu_\perp$ are the in-plane and out-of-plane Poisson's ratios.

S3. Diameter-dependent M-S bond identities in SW armchair and zigzag MS_2-NTs

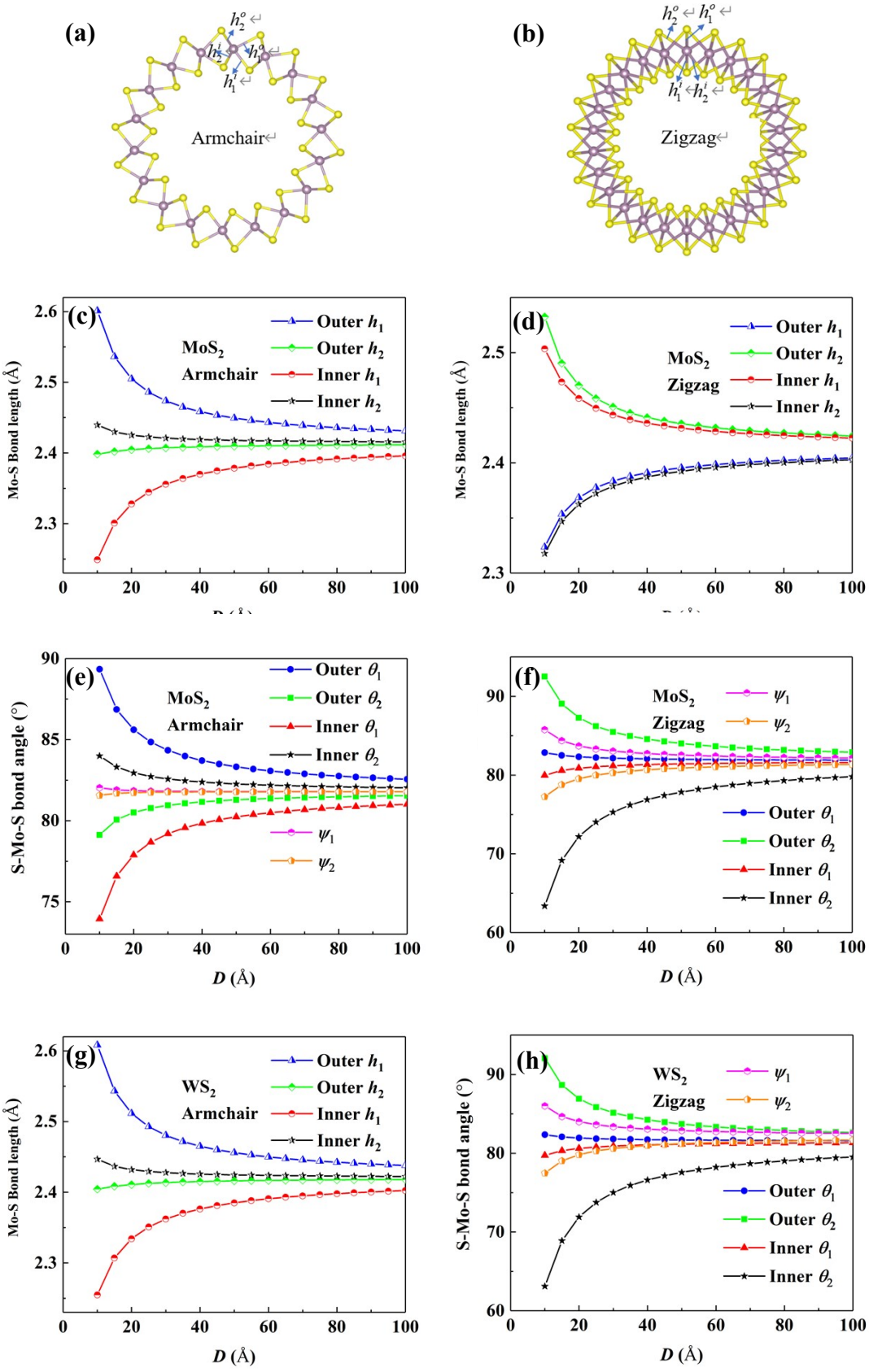

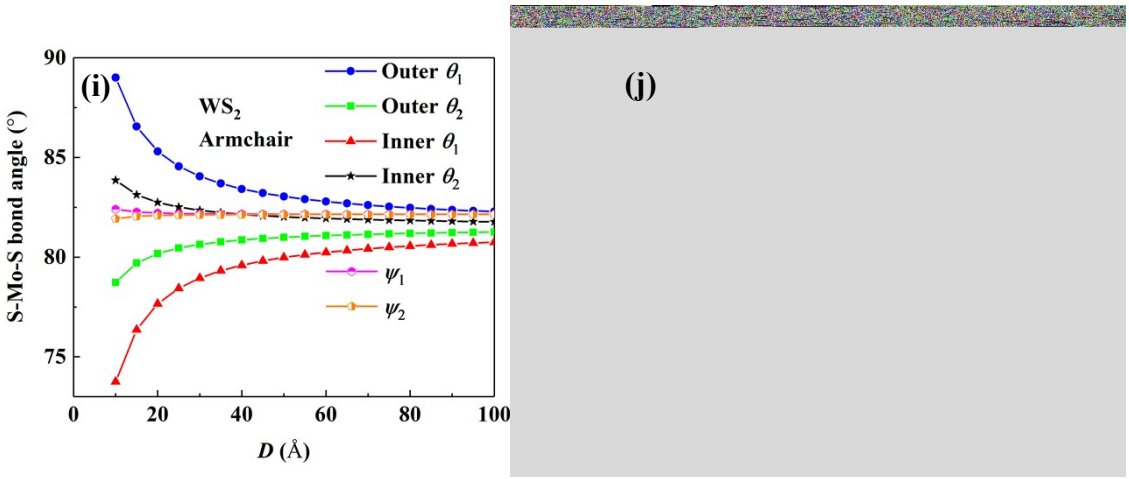

Figure S1. Top-views of structural configuration of SW armchair (a) and zigzag (b) MS_2-NTs. (c-j) Diameter-dependent M-S bond length and bond angles of armchair and zigzag MS_2-NTs.

Fig. S1(c-j) shows the bond identities (bond length and bond angle) of SW armchair and zigzag MS_2-NTs as a function of tube diameter. Notably, the change of bond identities shows an anisotropic property relative to chirality, while the trends of SW MoS_2- and WS_2-NTs are very similar as two materials have identical lattice structures.

S4. Band structures of monolayer MoS_2 and WS_2

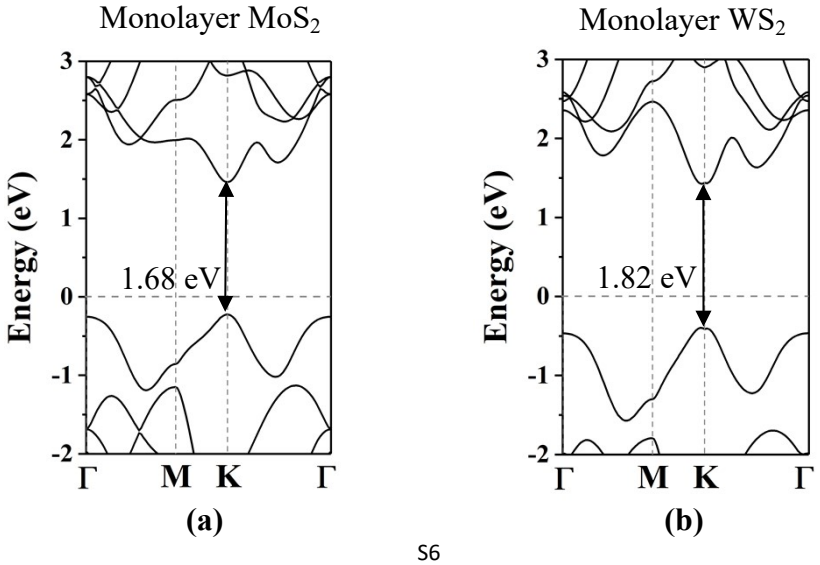

Figure S2. The band structures of monolayer (a) MoS_2 and (b) WS_2 are calculated by PBE method. It can be found that monolayer MoS_2 and WS_2 are the direct bandgap semiconductors with both VBM and CBM located at the **K** point of the first Brillouin zone.

S5. Partial density of states of SW armchair and zigzag MoS_2-NTs

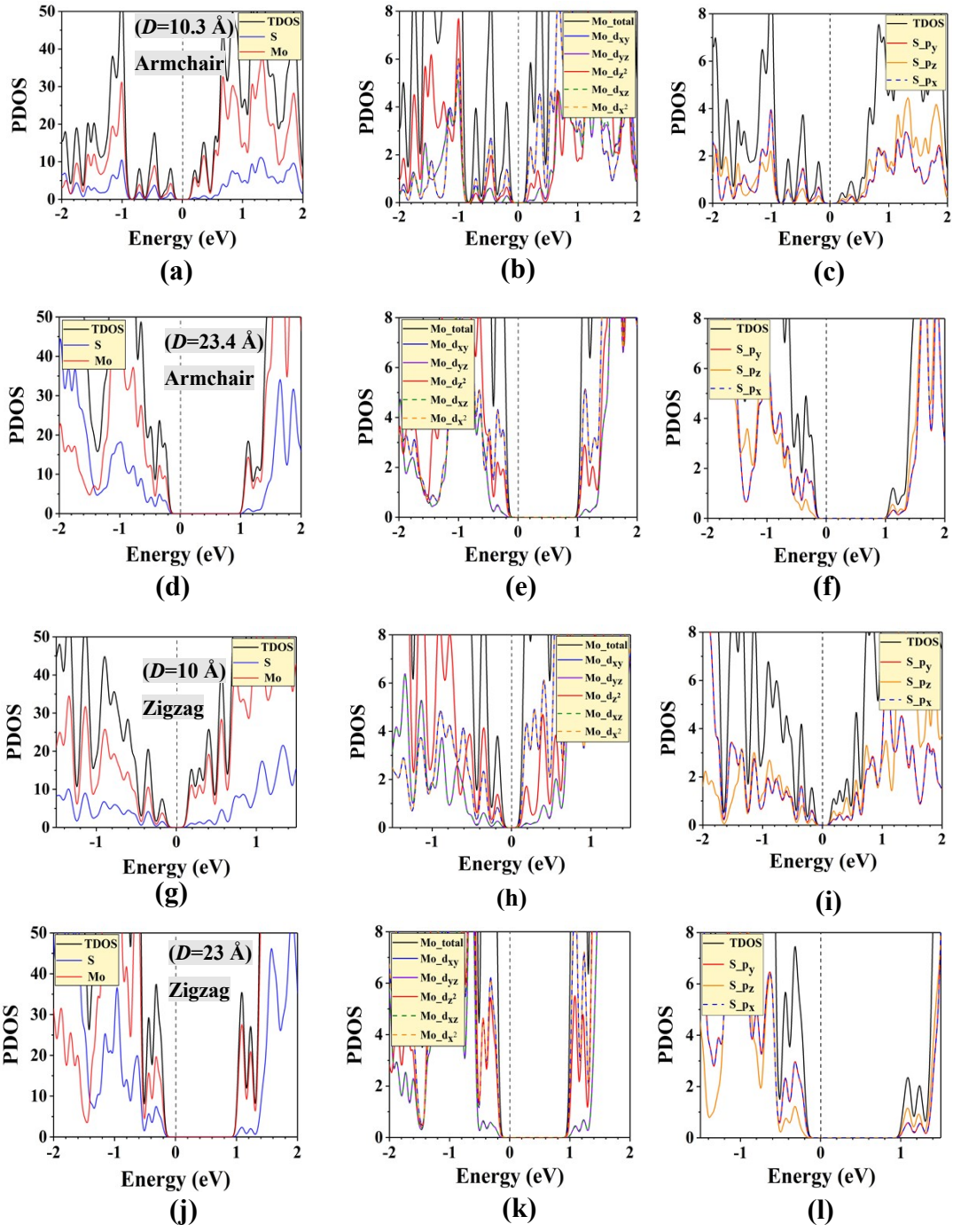

Figure S3. Partial density of states (PDOS) of SW armchair (a-h) and zigzag (g-l) MoS_2-NTs with different diameters. For the SW armchair and zigzag MoS_2-NTs, the CBM is mainly contributed by the Mo d_{xy}, d_{x^2} and d_{z^2} states, whereas the VBM is mainly from the Mo d_{xy}, d_{x^2}, d_{z^2} and S p_x, p_y states. The Fermi level is aligned to zero and indicated by vertical line.

S6. Phonon dispersion of SW MoS_2-NTs

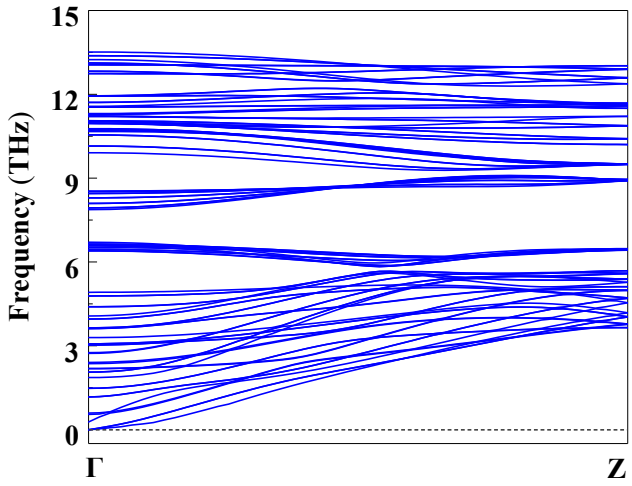

Figure S4. The phonon dispersion of SW armchair MoS_2-NTs with diameter of 1 nm. The phonon dispersion of SW MoS_2-NTs does not have negative frequencies in the Brillouin zone, suggesting the NTs is dynamically stable. The phonon spectrum is calculated by phonopy.

S7. Polarization of SW MoS_2-NTs

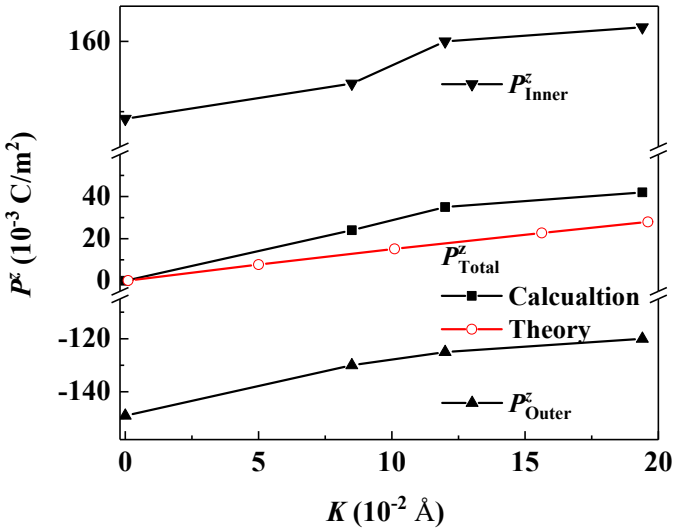

Figure S5. Evolution of polarization of SW MoS_2-NTs under different curvature. The black lines represent the results of DFT calculations, and the red line corresponds to the results of theoretical predictions.

Fig. S5 illustrates the polarization of SW MoS_2-NTs as a function of curvature. Notably, increasing the curvature of SW MoS_2-NTs will result in the reduction of polarization of outer part and the enhancement of polarization of inner part, which results in the total polarization increases with increasing curvature. Moreover, the trend of polarization obtained from DFT calculations is consistent with the change of theoretical predictions. Moreover, in the DFT calculations, we have considered the enhancement effect of the polarization caused by the charge transfer, resulting in the total polarization being larger than that of the theoretical predictions.

S8. Electron density of SW MoS_2-NTs

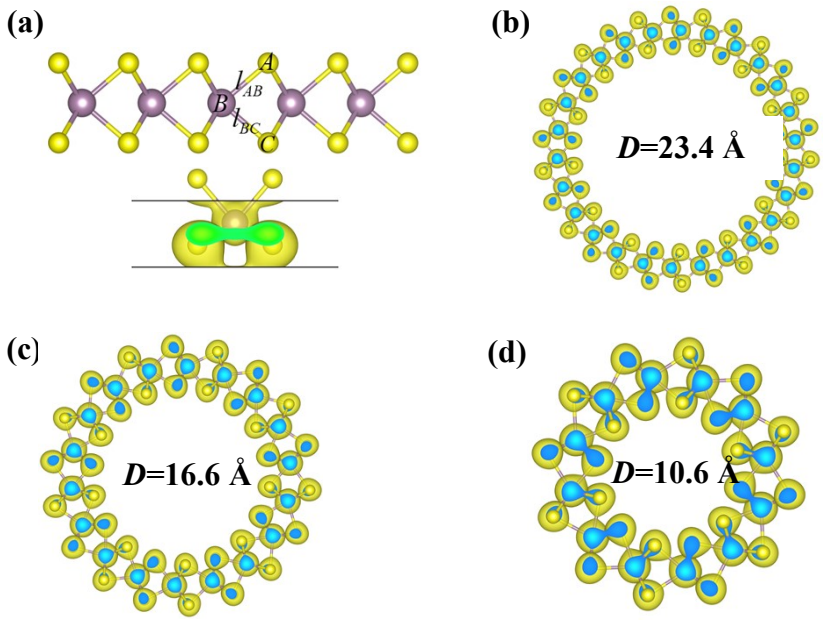

Figure S6. Evolution of contours of electron density of SW MoS_2-NTs under different diameters. The charge transfer caused by bending is obtained from Bader analysis.

S9. DW armchair MoS_2-NTs

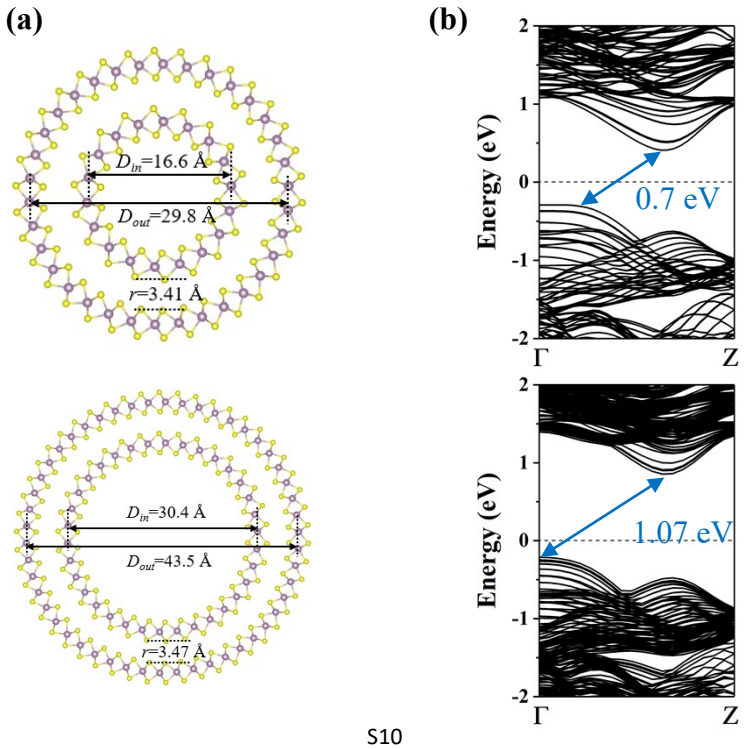

Figure S7. (a) Top-views of structural configuration and (b) projected band structures of DW armchair MoS_2-NTs with different diameters.

S10. Band alignment of inner and outer tubes in DW MS_2-NTs

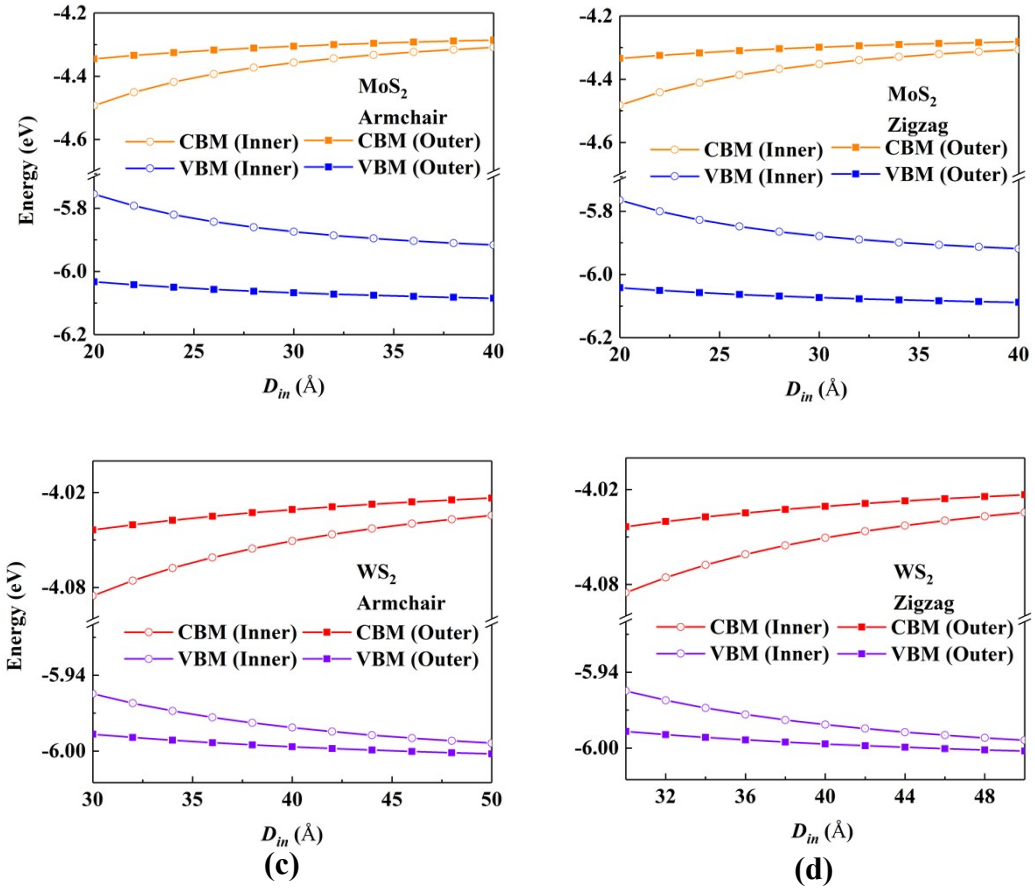

Figure S8. Band alignment of inner and outer tubes in DW MS_2-NTs with different diameters without considering flexoelectric effect. Due to the difference of bandgap between inner and outer tubes, a type I band alignment will take place.

S11. Evolution of band decomposed charge density of DW zigzag MoS_2-NTs

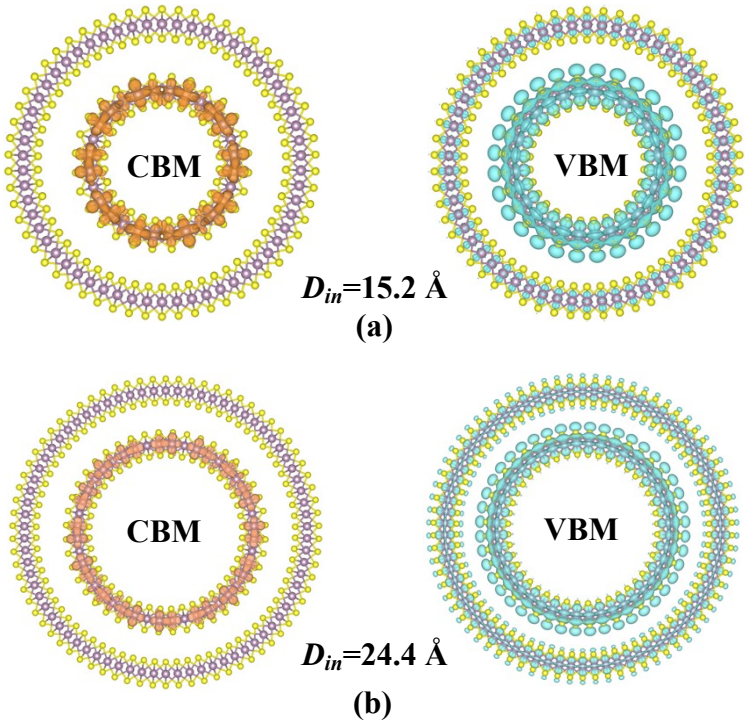

Figure S9. (a)-(b) DW zigzag MoS2-NTs with different diameters are calculated by DFT, where the band decomposed charge density indicating that the CBM states are always localized at the inner tube and the VBM states gradually shift from the inner to the outer as the diameter increases.

S12. Charge density difference in DW MoS_2-NTs

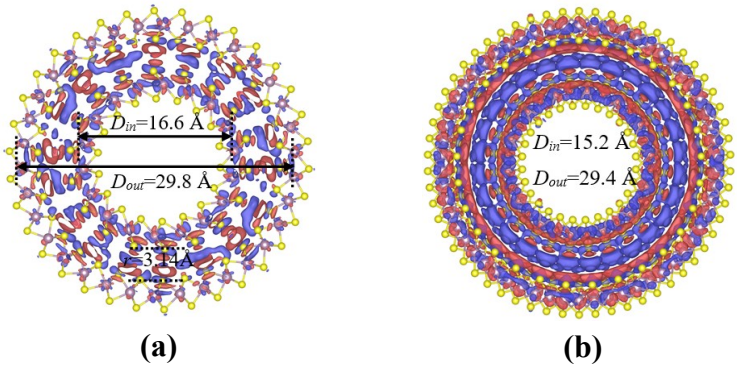

Figure S10. Plane-averaged charge density difference in DW (a) armchair and (b) zigzag MoS_2-NTs. Isocharge plot shows significant charge transfer from outer tube to inner tube. For the DW armchair MoS_2-NTs with the diameter of inner tube is 16.6 Å, the amount of transferred charge is 0.049282e. Similarly, when the diameter of inner tube is 15.2 Å，the amount of transferred charge of DW zigzag MoS_2-NTs is 0.048892e.

Table S1: The evolution of $\angle ABC$, bond lengths l_{AB}, l_{BC}, and the amount of transferred charges of Mo and S atoms in SW armchair MoS_2-NTs under different diameters.

Diameter (Å)	Monolayer	23.4	16.6	10.3
l_{AB} (Å)	2.41	2.49	2.53	2.64
l_{BC} (Å)	2.41	2.38	2.37	2.35
$\angle ABC$ (^{o})	82.4	81.7	79.1	76.8
ΔQ_A (e)	0	-0.047	-0.062	-0.074
ΔQ_B (e)	0	+0.015	+0.032	+0.041
ΔQ_C (e)	0	+0.022	+0.030	+0.033

S13. Spontaneous flexoelectricity and band engineering in MSe_2-NTs and MTe_2-NTs

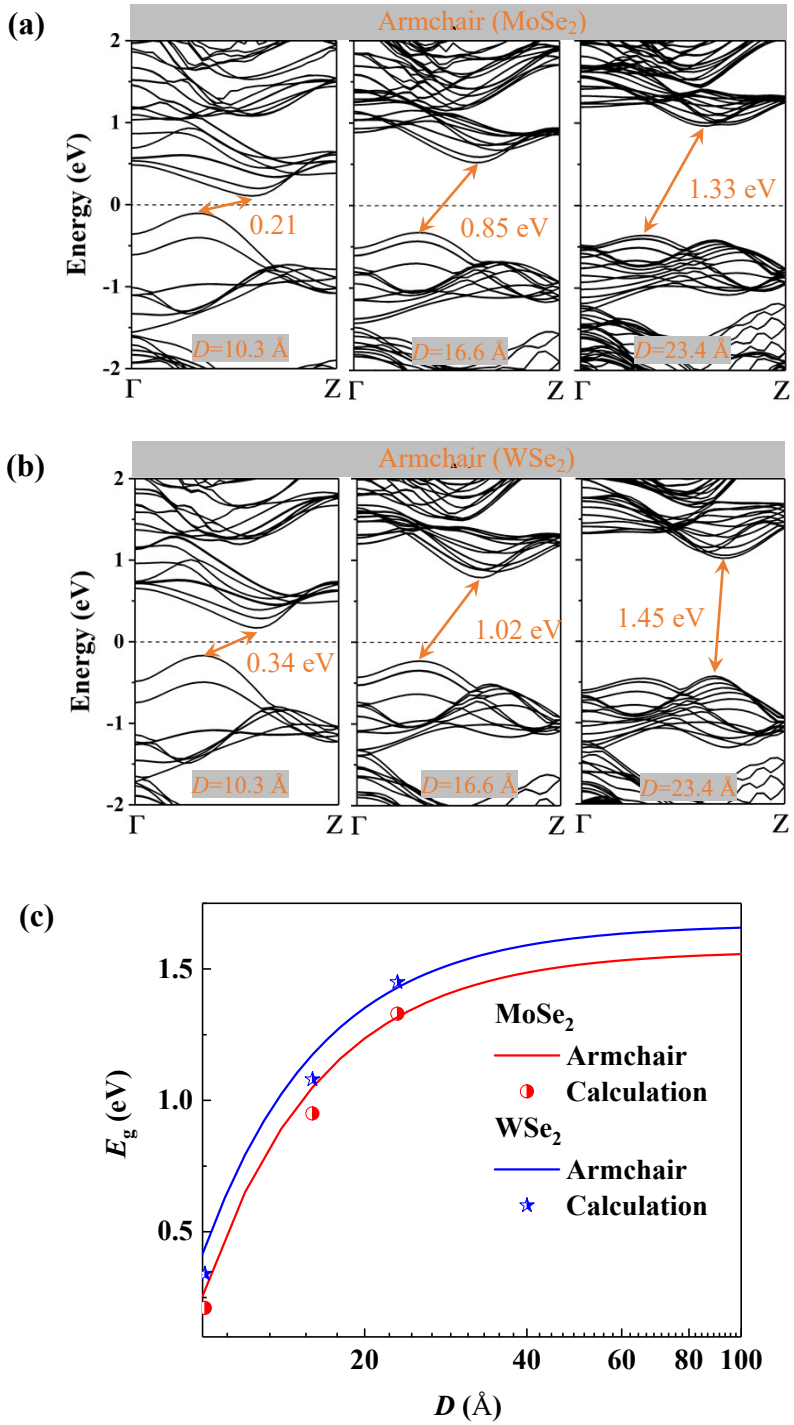

Figure S11. Band structures of SW armchair (a) $MoSe_2$- NTs and (b) WSe_2-NTs with different diameters. (c) Diameter-dependent bandgap of SW armchair MSe_2-NTs.

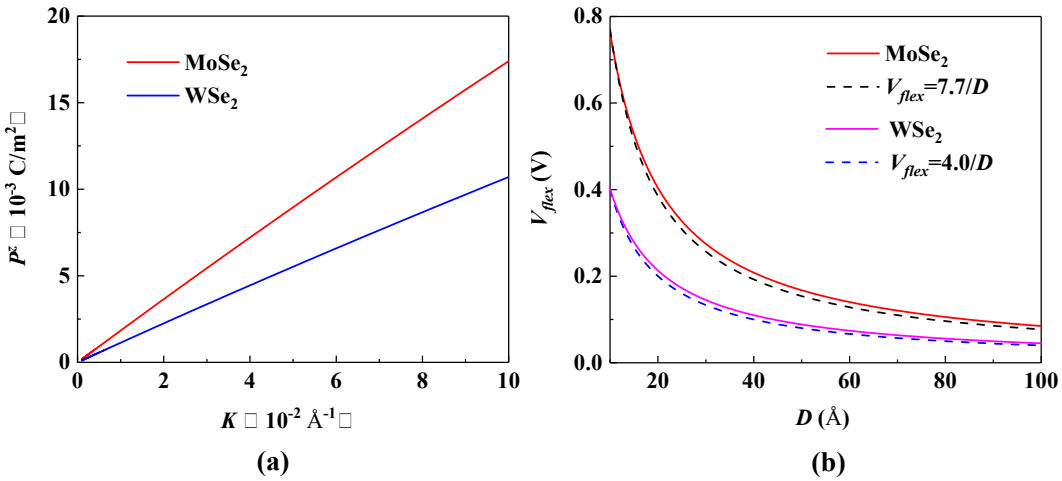

Figure S12. (a) Polarization P^z of SW MSe_2-NTs as a function of curvature. (b) Diameter-dependent flexoelectric voltage of SW MSe_2-NTs. The flexoelectric voltage in SW MSe_2-NTs follows the relation $V_{flex} = V_0 / D$. We obtain V_0 are the 7.7 VÅ and 4.0 VÅ for the SW $MoSe_2$- and WSe_2-NTs, respectively.

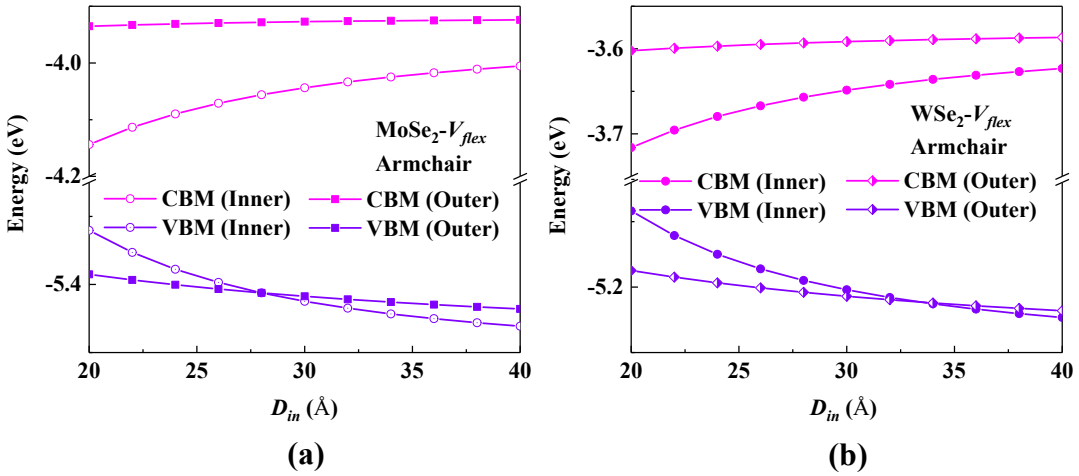

Figure S13. Evolutions of band alignment of inner and outer tubes in DW armchair (a) $MoSe_2$- and (b) WSe_2-NTs with different diameters. The threshold diameter is 2.8 and

3.3 nm for DW armchair $MoSe_2$- and WSe_2-NTs, respectively.

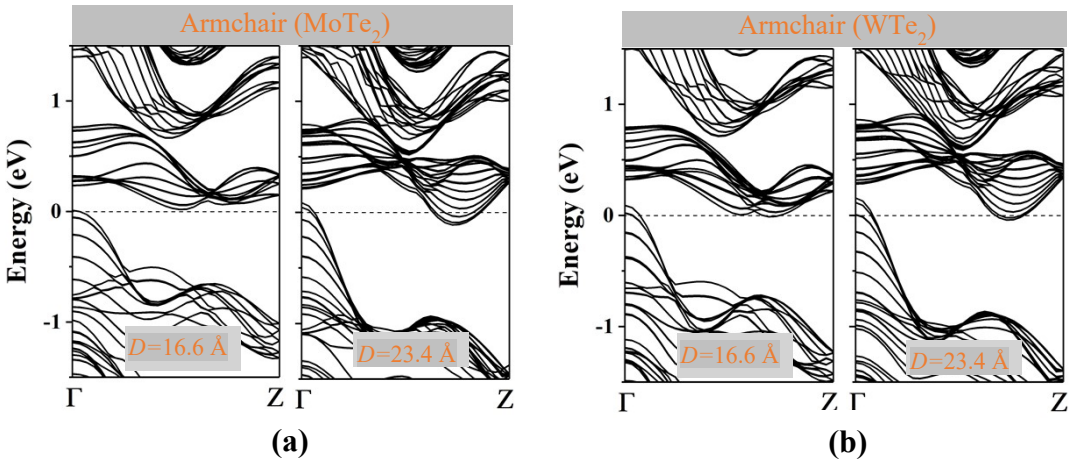

Figure S14. Band structures of SW armchair (a) $MoTe_2$- NTs and (b) WTe_2-NTs with different diameters.

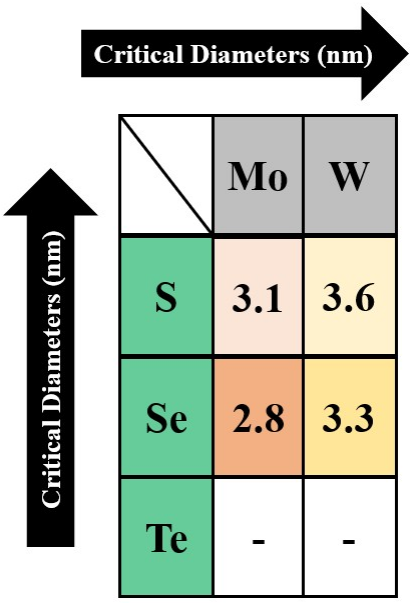

Figure S15. Trends in critical diameters of band alignment transition in DW MX_2-NTs, where M = Mo or W, and X = S, Se or Te.

Table S2. Input parameters for calculations of MSe_2-NTs. Lattice parameters a and thickness H,[1] anion partial electrostatic charges q_i,[2] cohesive energy E_C,[3] bandgap of monolayer E_g^b,[4] electron affinity of monolayer MSe_2 (χ),[1] effective mass of electron (m_e) and hole (m_h),[5] dielectric constants κ,[5] Poisson's ratio of in-plane (ν_P) and out-of-plane ($\nu_\perp$),[1] respectively.

	a (Å)	H (Å)	q_i (e)	E_C (eV)	E_g^b (eV)	χ (eV)	m_e (m_h) (m_0)	κ	ν_P($\nu_\perp$)
$MoSe_2$	3.32	3.35	0.71	2.30	1.57	3.87	0.7(0.55)	4.74	0.23(0.24)
WSe_2	3.32	3.36	0.49	3.21	1.67	3.53	0.53(0.52)	5.63	0.19(0.20)

References

1 J. Kang, S. Tongay, J. Zhou, J. B. Li and J. Q. Wu, *Appl. Phys. Lett.*, 2013, **102**, 012111.

2 K. H. Michel, D. Çakır, C. Sevik and F. M. Peeters, *Phys. Rev. B*, 2017, **95**, 125415.

3 Y. Liu, Y. Wang, M. Bo, X. J. Liu, X. X. Yang, Y. L. Huang and C. Q. Sun, *J. Phys. Chem. C*, 2015, **119**, 25071.

4 M. Zhang, J. Wu, Y. Zhu, D. O. Dumcenco, J. Hong, N. Mao, S. Deng, Y. Chen, Y. Yang, C. Jin, S. H. Chaki, Y. Huang, Jin Zhang and L. M. Xie, *ACS Nano* 2014, **8**, 7130-7137.

5 A. Ramasubramaniam, *Phys. Rev. B*, 2012, **86**, 115409.